Nonlinear transports and microvortex excitations in sheared quasi-two-dimensional dust Coulomb liquids

Wen-Tau Juan, Ming-Heng Chen, and Lin I
Department of Physics, National Central University, Chungli, Taiwan 32054, Republic of China
(Received 25 September 2000; revised manuscript received 12 March 2001; published 15 June 2001)

The microscopic spatiotemporal response of a quasi-two-dimensional dust Coulomb liquid to the shear induced by a cw laser is investigated through optical microscopy. The dust Coulomb liquid consists of many micrometer sized dust particles charged and suspended in a low pressure rf discharge background. Assisted by thermal fluctuations, the laser forcing enhances the cascaded generation of irregular vortices through reducing caging barriers for collective hopping. The vortex mixing leads to the mean velocity field with a simple structure that has a strong shear along the edge of the narrow laser beam. It also promotes the anomalous transverse diffusion with decaying strength from the line source. The viscosity and diffusion coefficient both show nonlinear dependence on the laser power under the interplay among the above nonlinear excitation and relaxation processes.

DOI: 10.1103/PhysRevE.64.016402 PACS number(s): 52.90.+z, 47.55.Kf, 66.10.Cb, 47.27.Nz

In a dusty plasma, the large negative charges on suspended dust particles can induce strong Coulomb coupling and turn the system into the crystal or liquid state with sub-mm interparticle distance [1–4]. Microscopic collective motions excited by thermal fluctuations, and by external drives such as laser beams and biased electrodes have been studied in the past few years [5–12]. Intershell motion in small circular dust clusters, and lattice waves in dust crystals are the few examples. Nevertheless, the spatiotemporal response of the dust Coulomb liquids to steady external shear forces is less well understood. In this work, this issue is addressed in a quasi-two-dimensional (2D) dust Coulomb liquid (2DDCL) suspended in a glow discharge.

Unlike the macroscopic fluids that exhibit smooth shear flows under moderate shears, our system operates at the discrete limit with strong mutual Coulomb interaction. It is an interesting many body system in which the microscopic particle motion can be directly monitored. In general, for nonequilibrium many body systems, many shear induced phenomena are originated from nonlinear particle interaction and rearrangement at the microscopic level [13]. The stick-slip type motions of the sheared molecular thin film between two solid surfaces and of granular systems are good examples [14,15]. In a crystal, the strong mutual coupling constrains particle motion in the caging barriers are formed by surrounding particles. It usually exhibits elastic deformation under a moderate external stress. On the other hand, thermal fluctuations in a stress-free liquid can induce collective particle hopping over the caging barrier [11]. The external stress further works with thermal fluctuations to promote particle hopping, and induces particle rearrangement [16]. The complicated excitation and relaxation of particle arrangement extending from the shear source to the remote area lead to the rich spatiotemporal response with nonlinear transports. In this study, these phenomena are explored experimentally in our 2DDCL stressed by a laser beam.

A laser beam can directly drive dust particle motion in the dusty plasma [5,6,8,10]. In our experiment, a liquid state with slightly disordered triangular cylinder structure that has vertical particle alignment can be formed in a weakly ionized low pressure discharge [2]. Particles along the same vertical chain tend to move together horizontally under thermal fluctuations. The motion of each chain in the horizontal plane can be optically tracked over long time. Namely, we have a quasi-2D system in which the microscopic spatiotemporal dynamical behaviors down to the particle excitation-relaxation time scale can be directly observed. We report the experimental observation of the enhanced vortex excitations originated from the shear line source by passing a narrow laser beam horizontally through the center of the suspended 2DDCL. It promotes anomalous persistent transverse diffusion with gradually decreasing strength from the laser line. The time averaged velocity field has a quite uniform structure with the largest velocity shear along the laser edges. The averaged viscosity and transverse diffusion coefficient both show nonlinear responses to the laser power.

The experiment is conducted in a cylindrical symmetric rf dusty plasma system described elsewhere [12]. A hollow coaxial cylinder with 3-cm inner diameter is put on the bottom electrode to confine the polystyrene particles (7 μm diameter) in the weakly ionized glow discharge ($n_e \sim 10^9$ cm^{-3}) generated in 250 mTorr Ar using a 14-MHz rf power system. Vertically, the suspended dust particles are aligned with eight particles for each chain by the vertical ion flow induced dipoles. There are 500 vertical chains confined and separated from the circular trap wall by a low pressure dark space (double layer). The particle (vertical chain) positions in the horizontal monolayer are monitored through an optical microscope. The dust mass and the dust charge are 1.9×10^{-10} g/dust and about $5000e$/dust respectively. The Debye length λ_D is between 100 and 200 μm and $a=310$ μm (a is the mean nearest particle separation). A cw Gaussian laser sheet (488 nm Ar^+ laser) with 0.4 mm half width and 2.5 mm height (covering the entire vertical chain) is introduced horizontally through the center of the floating circular dust cluster. The low pressure background provides small viscous damping to balance the energy flow from the shear source. The plasma operating parameters are fixed in the experiment.

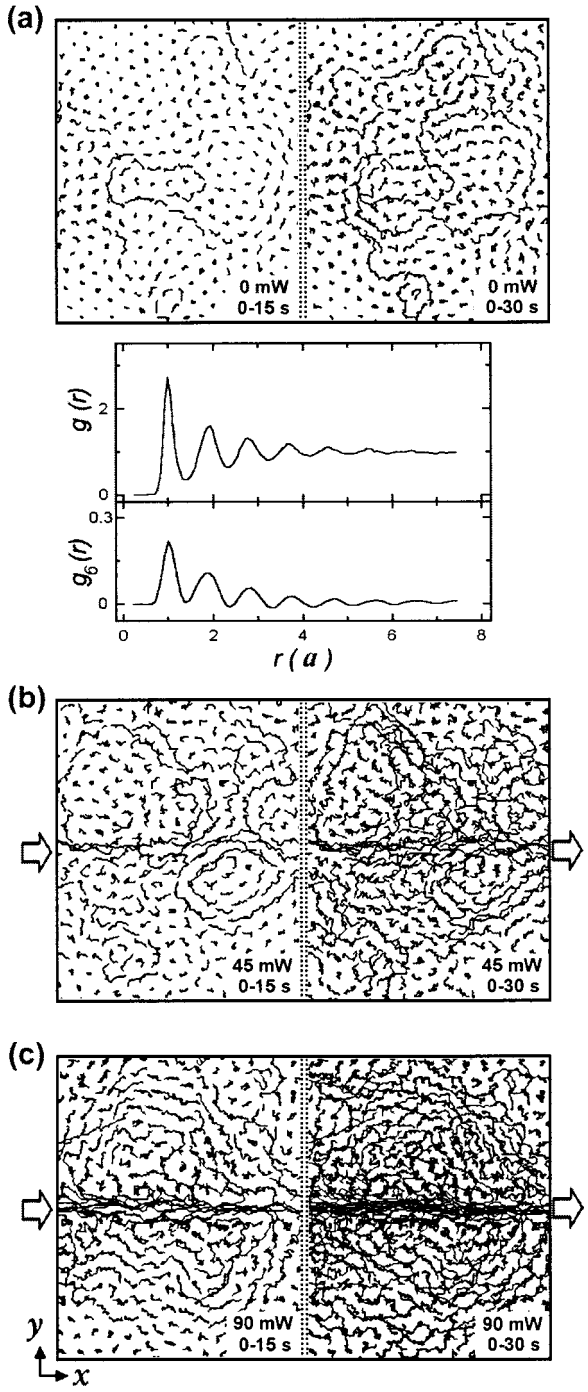

FIG. 1. (a) The particle trajectories with 15 and 30 s exposure times and the pair correlation functions $g(r)$ and $g_6(r)$ of particle positions and bond orientations respectively for the laser-free liquid state. The microvortices are generated by thermal assisted hoppings. (b) and (c) The particle trajectories with 15 and 30 s exposure times showing the laser enhanced vortex motions under 45 and 90 mW laser power. The trajectories are plotted at 3 Hz sampling rate. The arrows indicate the position and direction of the laser beam.

Figure 1(a) shows the particle trajectories with different exposure times, the pair correlation functions $g(r)$ and $g_6(r)$ for particle positions and bond orientation, respectively, for the state without laser forcing. $g(r)$ is the probability of finding another particle at radius r and $g_6(r) = \langle \psi_6(0)^* \psi_6(r) \rangle \times \psi_6(r) = (1/N_i) \Sigma_i \exp(i6\theta_i)$, θ_i is the angle of the vector from the particle at r to its ith nearest neighbor, and N_i is the number of the nearest neighbors. The system is in the cold liquid state melted from the triangular lattice structure. Unlike the crystal state, the absence of sharp peaks in $g(r)$ and the short correlation length for $g_6(r)$ associated with the distorted lattice lines manifest the loss of long range translational and orientational orders under thermal fluctuations. Dynamically, most of the particles exhibit small amplitude oscillations in the caging wells formed by their surrounding six nearest neighbors. Vortex-type collective hoppings over the barriers are occasionally excited by thermal fluctuations, which also deteriorate the lattice orientation. The hopping ceases when each particle travels about $1a$ and resettles in the new caging site [11]. Figure 1(b) and (c) show the trajectories with different exposure times and different laser power. The laser beam is introduced from left to right as indicated by the arrows. Introducing the external stress greatly enhances the formation of microvortices with gradually decaying intensity from the shear source to the remote region.

Figure 2(a) shows the time evolution of the particle velocity along x-direction averaged over the center 3.5 mm $\times 0.35$ mm zone along the laser driven region [i.e., $U_x(t)$], and the normalized enstrophies $\Psi_n(t)$ with and without the laser. Ψ_n is obtained by averaging the square of vorticity (i.e., the relative tangential velocity divided by the distance between two adjacent particle pair) over the whole plane except the laser zone. It measures the total intensity of the rotational excitations transferred to the region not directly driven by the laser. Increasing the laser power increases both the time averaged and the fluctuating levels of U_x and Ψ_n. Their fluctuations also show strong correlation. They both evidence the rotational excitations spreading from the laser line source to the rest area through the strong coupling between particles. Unlike in the linear response theory, the time averaged velocity $\overline{U_x}$ shows a nonlinear S-shape response to the laser power [Fig. 2(b)].

The vortex mixing makes the time averaged velocity field $\overline{V}(x,y)$ (over 750 s) exhibit a quite simple structure with the strongest shear along the edge of the laser beam, and a uniform small back flow in the rest area under the finite boundary [Fig. 3(a)]. The 2D plane is divided into many $1a \times 1a$ grids while measuring the averaged velocity field. Figure 3(b) shows that $\overline{V_x}(x=0,y)$ crosses zero at y between $1.7a$ and $2a$ (the coordinate origin is at the center of the system). This scale agrees with the mean radius of vortices around that region. The quite randomly distributed vortices along x direction makes the y component of the velocity at different points along the center y axis have a zero mean but larger fluctuations than the laser-off case. The mean shear rate nearby the laser boundary also shows an S-shape laser power dependence [Fig. 4(d)]. If we assume the stress intensity S is linearly proportional to the laser power, Fig. 4(e) shows that the viscosity, $\eta = S/\overline{U_x}$, is not a constant value. It is large in the low laser power regime and then drops down to a constant level in the high laser power regime.

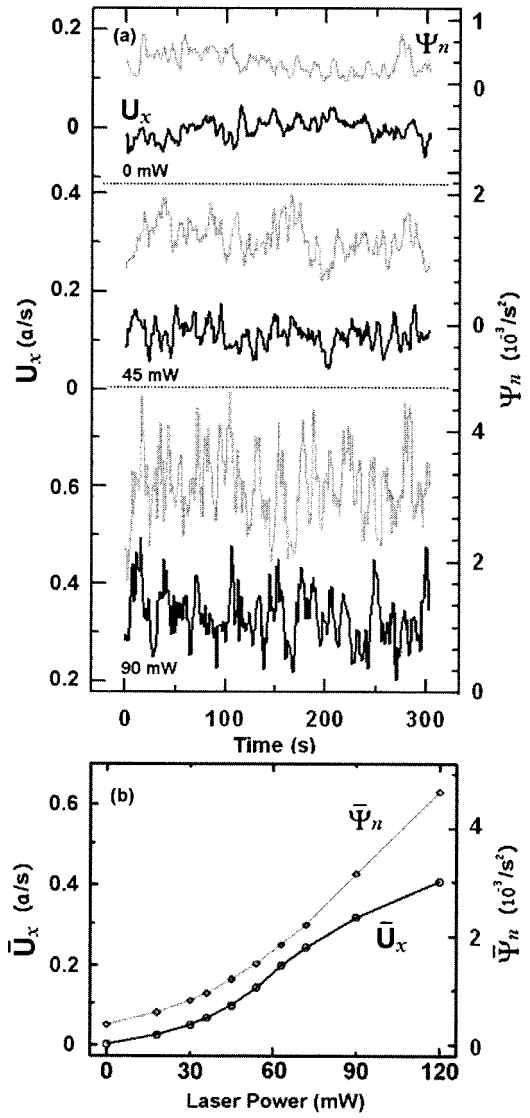

FIG. 2. (a) The time evolutions of the U_x (dark lines) and Ψ_n (gray lines) at different laser powers. (b) The laser power dependence of their time averaged levels $\overline{U_x}$ and $\overline{\Psi_n}$.

For the different points along the center y axis, the α direction components of the single particle mean square displacements (SMSD), $\langle \Delta R_\alpha^2(y,\tau)\rangle = \langle [R_\alpha(y,t+\tau) - R_\alpha(y,t)]^2\rangle \propto \tau^{H_\alpha(y)}$, under different laser powers are measured [Fig. 4(a), (b)]. $R_\alpha(y,t)$ is the α component of the particle position located at y at the starting time t. Note that $\langle \Delta R_y^2(\tau)\rangle/\tau$ is the transverse diffusion coefficient $D_y(\tau)$ measured with time interval τ [i.e., $\langle \Delta R_y^2(\tau)\rangle = \tau D_y(\tau)$]. Figure 4(c) shows that $\langle \Delta R_y^2\rangle$ at $\tau = 5$ s decreases with increasing y. Half width is about a few a. It indicates the vortex enhanced transverse diffusion with decaying intensity from the line source. Similar to the forward transport $\overline{U_x}$, the transverse diffusion coefficient at $y=0$ has an S-shape nonlinear dependence on laser power [Fig. 4(d)].

The SMSD vs time plots contain many interesting information about fluctuations and transports at different time scales. For the constant speed motion and random diffusion,

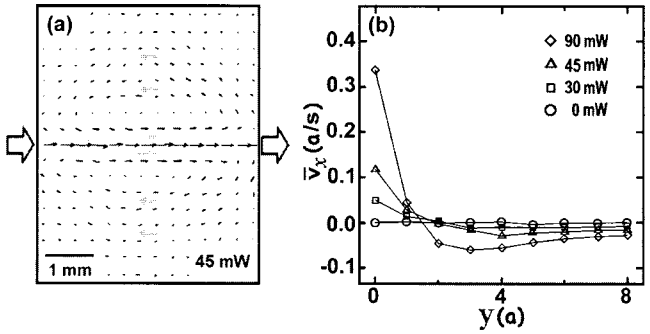

FIG. 3. (a) The mean velocity field averaged over 750 s. The 2D plane is divided into square boxes (each with $1a \times 1a$ size, where a is the mean nearest neighbor particle separation) for measuring the mean velocities of particles falling into the boxes. (b) The y dependence of the time-averaged velocity, $\overline{V_x}(x=0,y) = \langle R_x(t+\tau) - R_x(t)\rangle/\tau$ with $\tau = 5$ s, under different laser powers.

$H=2$ and 1 respectively. If the particle motion in a fluctuating background is not completely random and has a larger probability to follow (reverse) the direction of the last step, the diffusion is called persistent (antipersistent) with H greater (smaller) than 1 [17]. For the laser free case in the small τ regime (i.e., the high frequency motion), the thermally agitated particle is usually forced back to the center of the caging well by the surrounding particles [11,17,18]. It

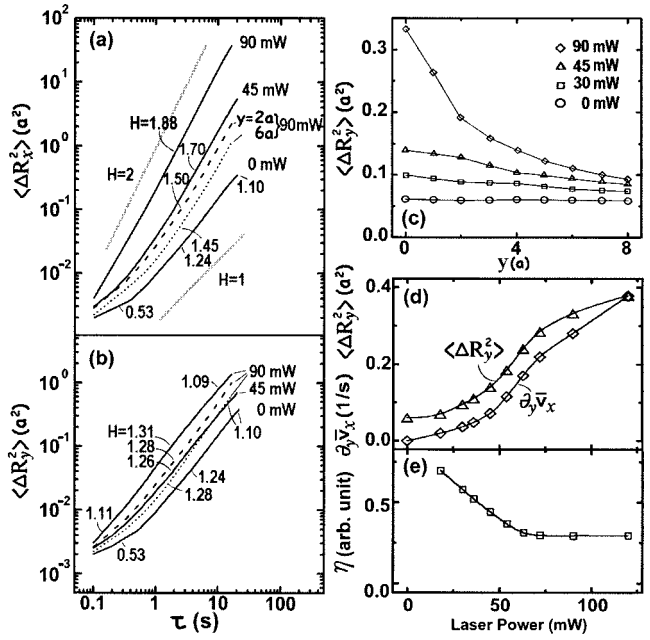

FIG. 4. (a) and (b) The time dependences of $\langle \Delta R_x^2 \rangle$ and $\langle \Delta R_y^2 \rangle$ for 0, 45, and 90 mW laser power. Solid lines, $y=0$; dashed and dotted lines, $y=2a$ and $y=6a$, respectively, at 90 mW laser power; gray lines, reference lines for $H=1$ and 2. The standard deviation for H_α is 0.03. At 0 mW, the curves for $\langle \Delta R_\alpha^2 \rangle$ are almost identical for $y<6a$ and only $\langle \Delta R_\alpha^2 \rangle$ at $y=0$ are plotted. (c) The y dependence of $\langle \Delta R_y^2 \rangle$ at $\tau = 5$ s under different laser powers. (d) The nonlinear laser power dependence of $\langle \Delta R_y^2 \rangle$ at $y=0$ and $\tau = 5$ and the shear rate $\partial_y \overline{V_x}(y=0.5a)$. (e) The laser power dependence of viscosity coefficient η.

makes $H<1$ [see the regime with $\tau<1$ sec in Fig. 4(a) and (b)]. Over a longer time interval, the displacement is dominated by the vortexlike hopping to neighboring sites. It switches to the persistent diffusion regime with $H>1$. Increasing the laser power causes the earlier onset of transition to the persistent regime and the larger $\langle \Delta R^2 \rangle$ for both x and y directions [Fig. 4(a) and 4(b)]. It manifests again the shear induced decaging effect.

The nonlinear response of η to the laser power is interesting. It is based on the assumption of the linear relation between the laser power and stress intensity, which might be an open question. In our experiment, the particles are transparent and absorb negligible light to heat up the background gas and causes thermal pressure effect. Introducing the laser beam also causes negligible changes of the local dust particle density and the shape of the entire cluster. The direct momentum transfer from the optical pressure could still play the major role on generating stress. The generic nonlinear responses of particle transports associated with microvortex excitations are supported by our recent computer simulation, regardless of the detailed particle interaction form [19]. In the low stress regime, η increases with the decreasing temperature. For the crystal case, η is infinite in the low stress regime until the stress reaches a threshold value to fluidize the crystal.

The observations can be reasonably explained by the thermal assisted mechanical instability [16]. For the cold crystal, particles sit in a periodic confining potential formed by the caging forces from the neighboring particles. They cannot exhibit hopping unless the stress reaches a threshold. In the stress-free cold liquid, thermal agitation can distort the caging potential through changing particle relative positions [18], transfer energy to particles, and induce vortexlike hopping over caging barriers [11]. Introducing an external stress breaks the symmetry and further promotes forward hoppings. In the low stress regime, the caging well is only slightly tilted. The hopping occurs but at a low rate. The motion is still strongly constrained by caging. It is the main cause for the large viscosity in Fig. 4(f) at low stress. Note that the viscosity in the cold 2D crystal is infinite at low stress [19]. Thermal fluctuation is thereby important to induce forward hopping. Increasing the stress level further promotes the hopping rate. Unlike merely tilting an 1D wash-board type caging potential, the extra transverse dimension makes the case more complicated. As shown in Fig. 5(a) with a short exposure time, vortices still occur in a stick-slip way at 45 mW laser power. The lattice lines for the liquid are usually bent and not lined up along the laser direction. The forward hopping can sometimes be jammed [e.g., in some section in the laser zone for the 7–15 s trajectories in Fig. 5(a)]. Assisted by thermal fluctuations, the stressed particles will find the easiest percolation paths for hopping, and branch off the laser zone. The particles enter a new slipping period. The vacancy left at the tail can be filled up by the trailing particles or by the particles in the neighborhood of the laser beam. Hopping vortices originated from the laser zone are thereby formed. Under the strong particle mutual interaction, these vortices quickly relax through cascaded excitations of new vortices with decaying strength in the remote region. The energy is eventually dissipated to the neutral gas background through the low pressure collisional drag.

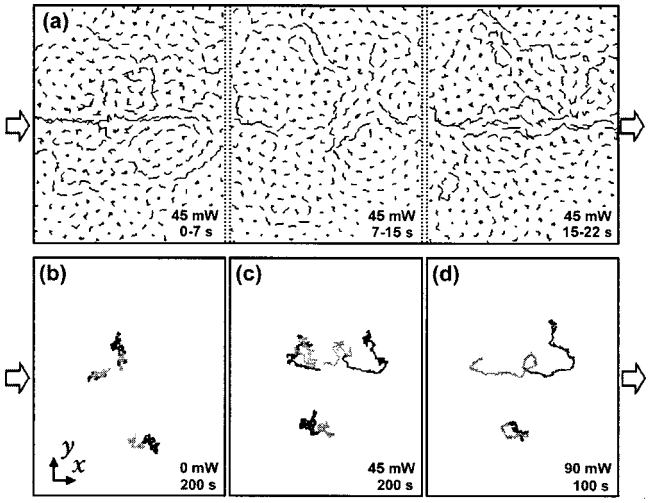

FIG. 5. (a) The sequential evolution of the particle trajectories at 45 mW laser power with short exposure times, which shows the stick-slip type excitation of shear enhanced hopping. The arrows indicate the position and the direction of the laser beam. (b), (c), and (d) The long time trajectories of a few typical particles at 0, 45, and 90 mW, respectively. The trajectories in the first and the second halves of the exposures are in gray and black, respectively. Note that in (b) and (c) there are two particles around the laser zone and the total exposure time is 200 s. In (d) there is only one particle around the laser zone and the total exposure time is 100 s.

Figure 5(b) and (c) show the typical long time (200 s) trajectories of three particles around the laser zone and a few a away from the laser zone at zero and 45 mW laser power respectively. Usually, the caged motion generates a clustered trajectory, and hopping generates a long thin trajectory. At zero laser power, the thin trajectories overlap with the clustered trajectories and are hard to identify. However, at 45 mW laser power, the trajectories show that particles can be sucked into the laser zone from the neighboring region, gain a fast forward speed and then branch off the laser zone. The alternate clustered and long thin trajectories again evidence that caging and hopping occur alternately, and the caging time is greatly shortened. Both the forward and transverse transports are enhanced. This also explains why $\overline{U_x}$ and $\langle \Delta R_y^2 \rangle$ at $y=0$ share the similar dependence on the laser power. The smaller excursion range of particles in the region away from the laser zone [e.g., Fig. 5(c)] also manifests again the lower transverse diffusion rate under the lower vortex intensity away from the laser zone.

In the high laser power regime (>80 mW), η decreases to a lower constant level and the diffusion rate reaches a high level. It evidences the significant suppression of the caging barrier. The initial caged regime with $H<1$ disappears for both $\langle \Delta R_x^2 \rangle$ and $\langle \Delta R_y^2 \rangle$ in the laser zone [e.g., at 90 mW, Fig. 4(a) and (b)]. The laser induced persistent motion dominates even at small τ. The typical higher speed motion of a particle in the laser zone at 90 mW laser power is shown in Fig. 5(d). However, even the long thin trajectory dominates, the motion is still not ballistic. The particles have chances to

branch off and reenter the laser zone. Namely, the laser driven particles are still irregularly dragged, through the accumulated interactions and cascaded vortices with other remote particles whose motions are affected by caging barriers [see, $H<1$ regimes at small τ for $\langle \Delta R_x^2 \rangle$ and $\langle \Delta R_y^2 \rangle$ at $y=2a$ and $6a$ in Fig. 4(a) and (b)]. It leads to the fluctuations in $U_x(t)$ and $\Psi_n(t)$ (Fig. 2), and makes $H_x(y=0)$ large [$H_x(y=0)=1.88$ at 90 mW] but still smaller than 2 [Fig. 4(a)]. Note that $H=2$ for a drift or a ballistic type motion with constant speeds. Also note that $H_y(y)$ only slightly increases from 1.24 ± 0.03 to 1.31 ± 0.03 as the laser power increases [Fig. 4(b)]. $H_y(y)$ enhanced by the stronger hopping is compensated by the more violent vortex mixing. The slight decrease of H_y closer to one for large τ (>10 s) is due to the randomly phased vortex generation and relaxation [11].

In conclusion, the experiment provides a microscopic picture of the generic spatiotemporal response to an external force of our quasi-2D liquid system in a low pressure background. The external stress and thermal agitation induce particle rearrangement through the generation of small irregular vortices from the line source. The strong mutual interaction further turns the directional driving into irregular particle motions through the cascaded generation of vortices with decaying intensity in the remote region. The work done by the laser stress is eventually dissipated to the low pressure gas background through the viscous drag. The vortex mixing leads to the averaged velocity field with a quite simple structure that has the strongest velocity shear in a narrow zone along the laser edge. It also enhances particle transverse diffusion with decaying strength from the line source. In the low laser power regime, the excitation is stick-slip type due to the caging effect. It causes the high viscosity and low transverse diffusion rate. In the high laser power regime, the caging barriers are more suppressed but the particle motions are still modulated by irregular vortex generation. The viscosity decreases to an almost constant level and the transverse diffusion rate increases.

This research is supported by the National Science Council of the Republic of China under Contract No. NSC-88-2112-M008-008.

[1] H. Ikezi, Phys. Rev. Lett. **42**, 1688 (1979).
[2] J.H. Chu and Lin I, Phys. Rev. Lett. **72**, 4009 (1994). Lin I, W.T. Juan, and C.H. Chiang, Science **272**, 1626 (1996).
[3] H. Thomas *et al.*, Phys. Rev. Lett. **73**, 652 (1994).
[4] Y. Hayashi and K. Tachibana, Jpn. J. Appl. Phys., Part 1 **33**, 804 (1994).
[5] M. Klindworth, A. Melzer, and A. Piel, Phys. Rev. B **61**, 8404 (2000).
[6] A. Homann, A. Melzer, and A. Piel, Phys. Rev. E **59**, R3835 (1999).
[7] A. Melzer, V.A. Schweigert, and A. Piel, Phys. Rev. Lett. **83**, 3194 (1999).
[8] S. Nunomura, D. Samsonov, and J. Goree, Phys. Rev. Lett. **84**, 5141 (2000).
[9] J.B. Pieper and J. Goree, Phys. Rev. Lett. **77**, 3137 (1996).
[10] W.H. Steal, D.A. Law, E. Tomme, B.M. Annaratone, and J. E. Allen, *XIV ESCAMPIG, Malahide, Ireland, 1998*, Vol. 22H, p. 114 (unpublished).
[11] C.H. Chiang and Lin I, Phys. Rev. Lett. **77**, 647 (1996); W.T. Juan and Lin I, *ibid.* **80**, 3073 (1998).
[12] W.T. Juan *et al.*, Phys. Rev. E **58**, R6947 (1998); W.T. Juan, *et al.*, Chin. J. Phys. (Taipei) **37**, 184 (1999).
[13] S. Granick, Phys. Today **52** (7), 26 (1999); G. Hahner and N. Spencer, *ibid.* **51** (9), 22 (1998).
[14] P.A. Thompson and M.O. Robbins, Science **250**, 792 (1990).
[15] S. Nasuno, A. Kudrolli, and J.P. Gollub, Phys. Rev. Lett. **79**, 949 (1997).
[16] D.L. Malandro and D.J. Lacks, Phys. Rev. Lett. **81**, 5576 (1998).
[17] J. Klafter, M.F. Shlesinger, and G. Zumofen, Phys. Today **49** (2), 33 (1995).
[18] F.H. Stillinger, Science **267**, 1935 (1995).
[19] W. T. Juan and Lin I (unpublished).